A Compact and Reconfigurable Dual-Mode Configuration Substrate Integrated Waveguide Dual-Band Bandpass Filter for 5G and Millimeter-Wave Communications

Zahid A. Bhat[1], Javaid A. Sheikh[1, *], Sharief D. Khan[2], Ishfaq Bashir[1], and Raqeebur Rehman[1]

Abstract—In this paper, a compact and reconfigurable rectangular substrate integrated waveguide structure dual-mode configuration dual-band bandpass filter has been presented for modern day 5G communication and millimeter-waves. The dual-band bandpass filter is realized by utilizing the two pairs of dumbbell-shaped defected ground structure. The dumbbell-shaped defected ground structures etched on both the ground and the top side of the cavity have been used to produce transmission zeros, minimize the circuit size, and enhance the passband characteristics at a particular frequency of operations. In an effort to demonstrate the proposed dual-band substrate integrated waveguide bandpass filter, this configuration has been designed and fabricated at the 28.3 GHz and 38.5 GHz frequency using low-cost PCB technique. The centre frequency of the second passband has been easily tuned using the geometrical parameters of the filter to achieve the desired applications in the 5G frequency band. Furthermore, the measured in-band return loss (rejection attenuation) of the two bands is approximately better than 26 dB and 28 dB, respectively. The insertion loss of not more than 01 dB for both bands of the filter has been achieved. This dual-band filter operating at the licensed frequencies for the 5G spectrum bands renders this filter appropriate for numerous 5G and millimeter-wave communication applications.

1. INTRODUCTION

The fifth generation (5G) mobile communication system delivering high-speed has attracted worldwide attention. Filter being one of the key components of the modern wireless communication systems, its performance will have a significant impact on the whole system's performance. For this reason, it has become the research hotspot in microwave and millimeter-wave (mm-Wave) field. Substrate integrated waveguides (SIWs) have been developed as a promising and prominent technology for the 5G mobile communication systems over the years. These waveguides offer distinctive advantages in the design of mm-Wave [1, 2] and microwave devices [3], and has attracted more and more attention in the modern-day research practices. In highly diverse geographic and high-density populated countries like India and China, high capacity and coverage demands are increasing day by day [4], so it has become imperative to use the multiband operation in the upcoming 5G mobile communications to meet these requirements [5]. In addition, the necessities of the components are that the devices should be of low-cost with low-losses, compact and easily integrable with the components of the modern-day wireless communication systems or planar technology. Numerous factors like low-cost, high-quality factor, and the easy integration of a dual-band SIW BPF with the planar technology devices make them the potential candidates for the

5G future generation systems. Several structures and prototypes have been developed to design these favourable dual-band BPFs using SIW technology in the recent years.

To attain the operation of dual-band, [6] reports a dual-band BPF that utilizes the advantage of TE_{102} and TE_{201} modes (degenerate modes) of a large structure SIW cavity which hampers the theory of the integrated circuits. In [7–9], complementary split ring resonators (CSRRs) stacked SIW cavities have been investigated and researched for the miniaturization process of the SIW based filter designs. SIWs have also been utilized to design and fabricate millimeter-wave filters [10, 11]. The use of transparent graphene to design a dual-band microstrip filter for the future 5G applications has also been proposed in [12], but the application of the filter is limited because of large insertion loss. The size/dimensions of the components is also the concern that limits the application of the filters for the 5G communication systems. In [13], a dual-band BPF has been fabricated and designed utilizing the multimode characteristics of the SIW, but the size is comparatively large to support the devices operating at 5G frequency band. Moreover, to form the resonance structures and minimize the circuit size, defected ground structures (DGSs) have been widely used which also improve the stopband characteristics of the filter [14, 15]. Although an appreciable amount of work has been reported in this regard, to our knowledge not much of the work has been reported using a DGS at mm-Wave band of frequency [16–23].

This paper discusses a simple and novel dual-band BPF that employs the multi-mode properties of SIWs proposed for the modern 5G and mm-Wave communication systems. This dual-band BPF combines all the advantages and disregards the disadvantages by utilizing dumbbell-shaped DGSs (DB-DGSs) etched on the ground side and top side of the SIW cavity to produce transmission zeros, minimize the circuit size, and enhance the passband characteristics at a particular frequency of operations. To validate the operation of proposed SIW based dual-band filtering operating at the frequencies of 28.3 GHz and 38.5 GHz, the filter has been designed, fabricated, and measured. It has been observed that the filter attains a high inter-band isolation, good skirt selectivity, good spurious response, compactness in terms of size, and a good agreement in terms of simulated and measured results.

2. DESIGN OF DUAL-BAND FILTER

The resources of frequency spectrum are becoming highly crowded with the speedy development of current and modern-day wireless communication systems, and a single-band BPF cannot comply with the requirements of precise spectrum division, which is the reason that multi-band BPFs are increasingly becoming a hotspot of the scientific explorations and researches. The proposed dual-band BPF is realized by using a DB-DGS SIW structure. The substrate material used to fabricate and design the dual-band BPF is Rogers RT/Duroid 5880 having the thickness (h) of 10 mils with the values of loss tangent ($\tan\delta$) and dielectric constant (ε_r) as 0.0009 and 2.2, respectively.

2.1. Design and Analysis of the Filter

Figure 1(a) shows the basic cavity configuration and design of the SIW. It has been observed that the leakage flanked by the via-holes of the SIW is negligible only once the distance between the neighbouring via-holes is less than one-fifth of the guided wavelength, i.e., $P < \lambda_g/5$, and the diameter of a via-hole is less than one-fourth of the P, i.e., $D < P/4$, where λ_g is the guided wavelength. The equivalent rectangular waveguide length (L_{eqv}) and width (W_{eqv}) are supposed as the length (L) and width (W) of the SIW, and this is calculated using Equation (1):

$$L_{eqv} = L - \frac{D^2}{0.95P}, \quad W_{eqv} = W - \frac{D^2}{0.95P} \tag{1}$$

The guided wavelength (λ_g) and the corresponding cut-off frequency (f_c) are calculated using Equations (2) and (3) [16].

$$\lambda_g = \frac{c_o}{f_c\sqrt{\varepsilon_r}} \tag{2}$$

$$f_c = \frac{c_o}{2W_{eqv}\sqrt{\varepsilon_r}} \tag{3}$$

where ε_r is the physical parameter of the material substrate, and c_o is the free-space velocity of the light [16]. It can be observed that Equation (3) states how f_c decreases with the increase in the width (W_{eqv}/W) of the cavity. The same relation between L and the filter's resonance frequencies can be understood and modelled by utilizing the High Frequency Simulating Structure (HFSS) v.15 as illustrated in Fig. 1(b). It can be understood that varying the length (L) of the SIW cavity from 7 mm to 10 mm, the fundamental frequency, i.e., f_0, remains almost unchanged while the second frequency varies from 35 GHz to 38 GHz. Moreover, it is also illustrated that the length L affects the second frequency while it is less effective on the fundamental frequency.

(a)

(b)
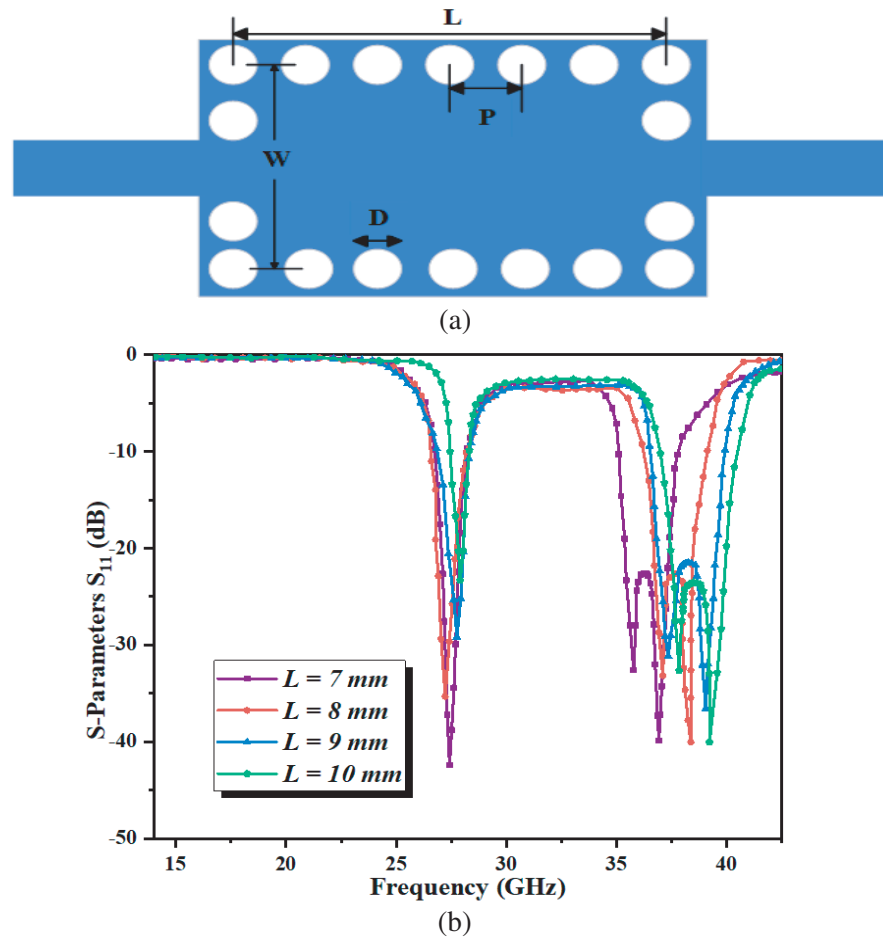
Figure 1. (a) The top-view of the simple SIW structure. (b) The relation between the S-parameters (S_{11}) and the length (L) of the SIW.

## 2.2. The Characteristics and Structure of SIW with its Dumbbell Slots

Figure 2 shows the proposed dual-band SIW filter having top and bottom sides etched with DGSs which defines the new method of miniaturization of the SIW filters. It consists of the main SIW based cavity resonator connected via the microstrip lines of 50 Ω and the DB-DGSs that are etched on the ground and top side of the SIW resonator. The magnetic coupling interfaces formed by via-holes are extremely small to be fabricated at such high frequency, and it is very hard to use such type of coupling to design the SIW filters for millimeter-waves. The DB-DGSs have been widely used, a familiar method to implement and design the low-pass filter with the purpose of producing the transmission zeros and cut-off frequency (f_c) at the upper side of stopbands. To easily design and analyse the DGS, an equivalent LC circuit can be used to represent it [17]. However, because of certain limitations there are very few research papers
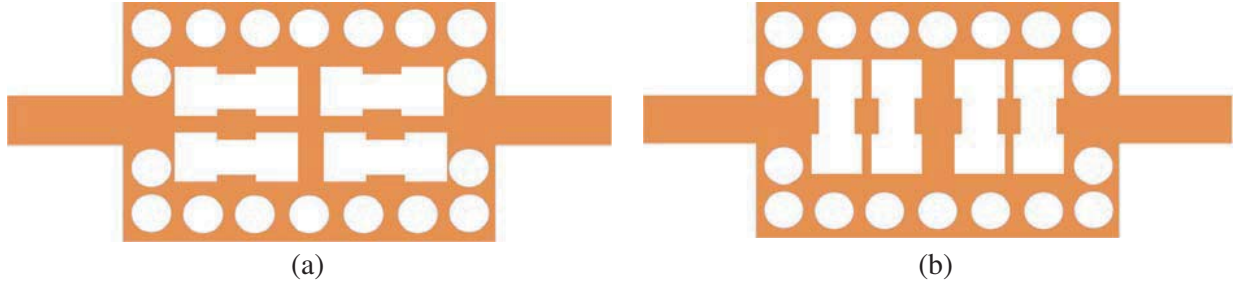
Figure 2. The proposed structure of dual-band SIW based filter. (a) The top metal plane, and (b) the bottom metal plane.

in which DB-DGS have been used to design the millimeter-wave devices.

The proposed filter has been designed using the substrate material of Rogers/RT Duroid 5880 having the dielectric constant (ε_r) of 2.2 and the corresponding thickness of 10 mil. Two pairs of dumbbell slots of equal size are etched on the ground and top metal planes of the SIW resonator. The slots engraved on the top side of the metal plane are placed in perpendicular direction to the slots of the bottom plane. The proposed dual-band filter can produce two resonances at the second frequency passband and the transmission zeros between the two bands. The magnetic field distribution of this dual-band mm-Wave filter for the resonant modes TE$_{101}$ and TE$_{102}$ is presented in Fig. 3.
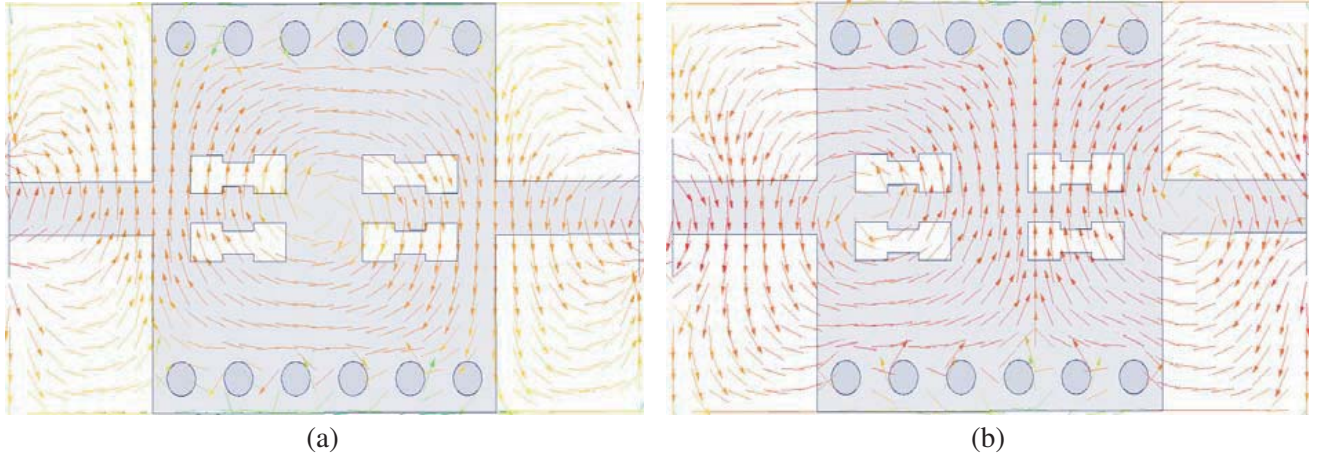
Figure 3. The H-field distribution of designed dual-band mm-Wave filter. (a) TE$_{101}$ mode. (b) TE$_{102}$ mode.

Figure 4 shows the streamlines formed by the poynting vector which clearly shows the proper flow of energy from port 1 to port 2 and vice-versa.

A dual-band mm-Wave BPF has been implemented and designed by taking advantage of the proposed SIW section with the pair of etched slots. From Equation (2), it is clearly understood that increasing the value of the width (W) results in the shrinkage of the stopband between the two passbands, which is illustrated in the Fig. 5. The LC equivalent circuit of the DGS resonance structures makes it more convenient and easier to analyse the proposed and designed dual-band BPF. Fig. 6 displays the equivalent circuit model of the proposed SIW dual-band mm-Wave BPF, wherein the 1st and 3rd sections of the circuit represent the SIW segments on the left and right sides of the slots, respectively. The 2nd section of the circuit represents the DGS, i.e., the slotted section of the proposed filter. In the 2nd section, the capacitance C$_1$ reinstates the capacitance which is created by the corresponding gap in between the slotted elements on the ground and top metal planes. C$_{r2}$ and L$_{r2}$ replace the capacitance and inductance developed by the engraved slots on the ground and top planes of the filter.

(a)

(b)
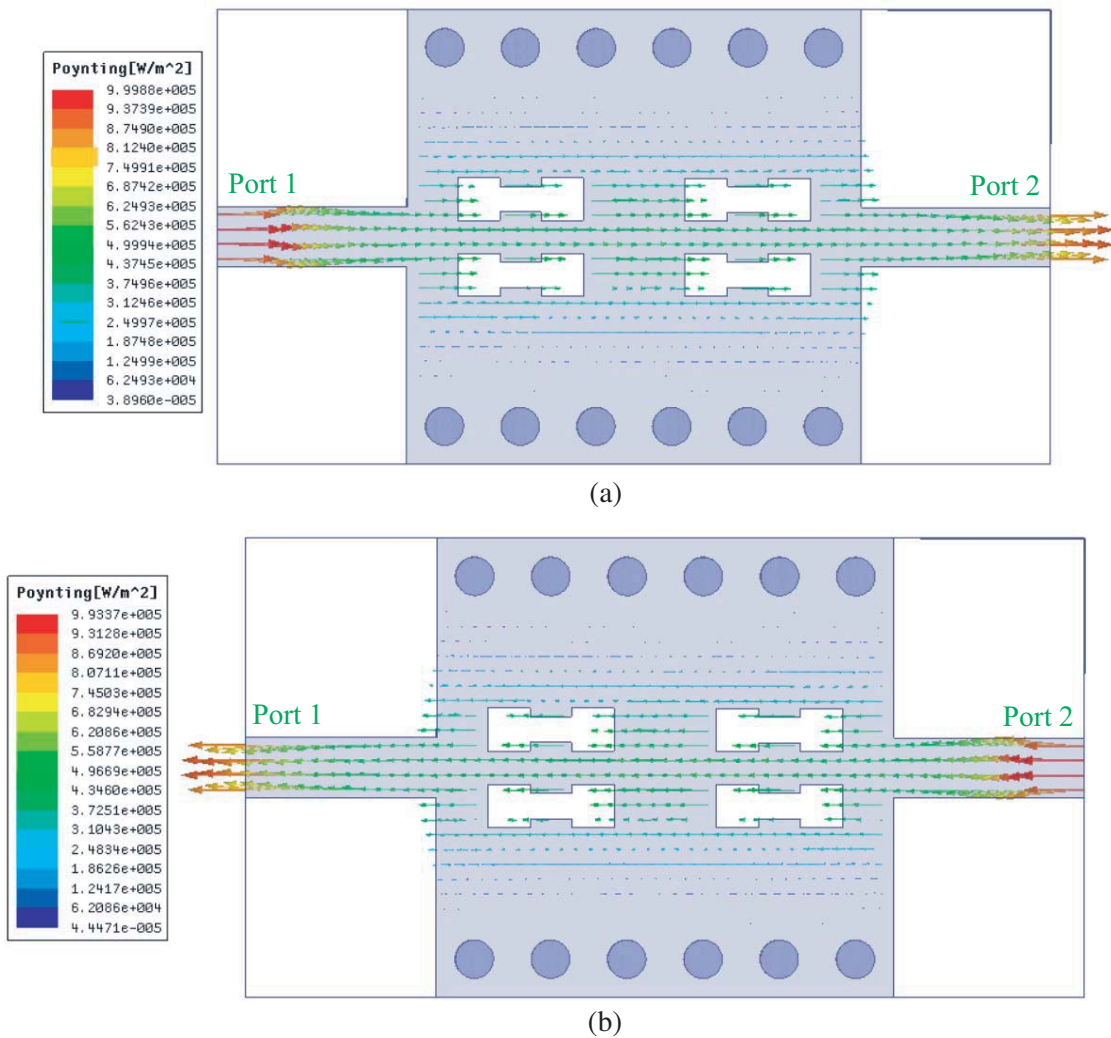
Figure 4. The streamlined plot of the poynting vector. (a) When port 1 is excited, and (b) when port 2 is excited.

The reactance of the equivalent circuit in the 2nd section is calculated as:

$$jX_r = j\frac{\omega^2 L_{r2}\left(2C_{r2} + C_1\right) - 2}{\omega C_1 \left(1 - \omega^2 L_{r2}C_{r2}\right)} \tag{4}$$

Equation (4) helps to derive the resonant angular frequency (ω) and the corresponding anti-resonant angular frequency (ω_k). It has been studied in [18] that when the reactance (jX_r) is zero $(jX_r = 0)$, the resonant frequency follows. Similarly, once the reactance (jX_r) is infinite $(jX_r = \infty)$, the anti-resonant frequency follows. While both the sections of SIWs in the equivalent circuit generate only the reactance frequencies. Mathematically, the relation between the resonant conditions and the equivalent LC circuit parameters can be derived in the same way as in [18].
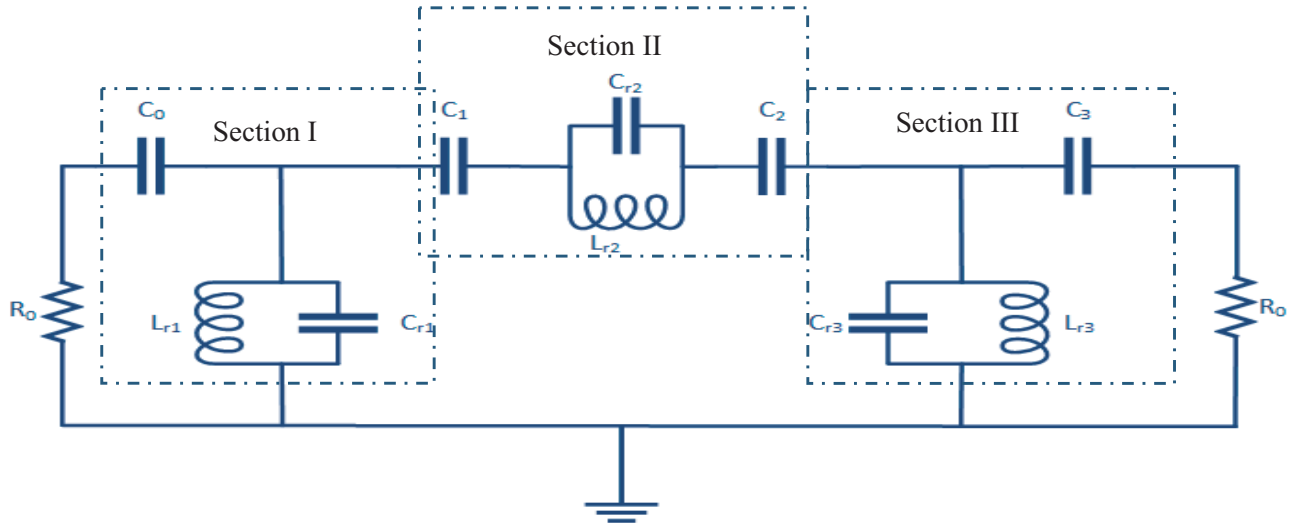
When $jX_r = 0$,

$$\omega_0^2 = \frac{2\omega_k^2 C_{r2}}{2C_{r2} + C_1}, \quad \frac{1}{C_{r2}} = \frac{2}{C_1}\left(\frac{\omega_k^2}{\omega_0^2} - 1\right). \tag{5}$$

When $jX_r = \infty$,

$$\omega_h^2 = \frac{1}{L_{r2}C_{r2}}, \quad L_{r2} = \frac{1}{\omega_h^2 C_{r2}} \tag{6}$$
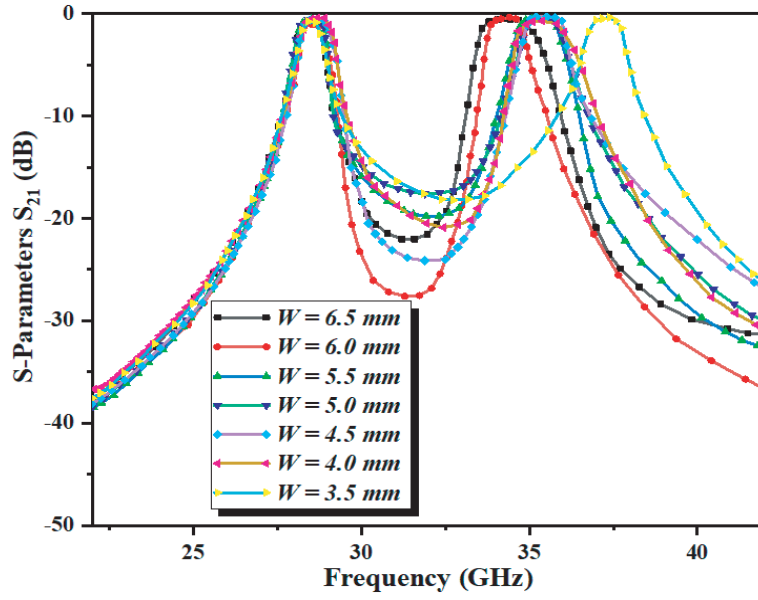
Figure 5. The S-parameters of the proposed dual-band mm-wave BPF for different values of the width (W).


Figure 6. The LC equivalent circuit model of the proposed dual-band filter.

where ω and ω_h are the frequencies of the attenuation poles and transmission zeros, respectively.

The Rogers substrate material RT/Duroid 5880 having the dielectric constant (ε_r) of 2.2 with the loss tangent of 0.0009 and thickness (h) of 10 mils has been utilized to design the mm-Wave dual-band BPF. The absolute dimensions for the proposed dual-band BPF obtained in Ansoft HFSS are as follows: $L = 10\,\text{mm}$, $S = 1\,\text{mm}$, $D = 0.5\,\text{mm}$, $W = 6.5\,\text{mm}$, $W = 0.752$, $L_{s1} = W_{s1} = 0.56\,\text{mm}$, $L_{s2} = 0.54$, $W_{s2} = 0.38$. It is clearly reflected in Fig. 5 that the cut-off frequency of the first band is pratically constant whereas varying the width (W) of the SIW waveguide, the centre frequency of the 2nd band can be tuned or controlled for preferred applications.

3. EXPERIMENTAL AND MEASURED RESULTS

For demonstration, the proposed dual-band mm-Wave BPF shown in Fig. 1 has been designed and fabricated on the Rogers substrate material RT/Duroid 5880 having the thickness (h) of $0.254\,\mathrm{mm}$, dielectric constant (ε_r) of 2.2 with a loss tangent of 0.0009. The photographic views of the top and bottom sides of the fabricated dual-band mm-wave BPF are illustrated in Fig. 7(a) and Fig. 7(b), respectively. The comparison of the simulated results accomplished by using the Ansys HFSS v15 software and the measured results realised using the Agilent E8364Cnetwork analyser is displayed in Fig. 8. In order to examine the details of in-band performances, Fig. 8 clearly depicts the two upper-band transmission poles in the passband of the mm-Wave filter with three transmission zeros in the stopband. The in-band attenuations (return losses) measured for the two bands are approximately better than $26\,\mathrm{dB}$ and $28\,\mathrm{dB}$, respectively. Furthermore, the insertion loss of less than $01\,\mathrm{dB}$ for the both bands of the filter has been achieved. The measured and simulated results show that they are in good agreement with one another, and the difference between them is because of the fabrication tolerance and dielectric loss. Table 1 shows the detailed comparison between the already existing and proposed filters. From the table it is clear that the proposed scheme outperforms the exiting schemes in terms of desired parameters.

(a)   (b)
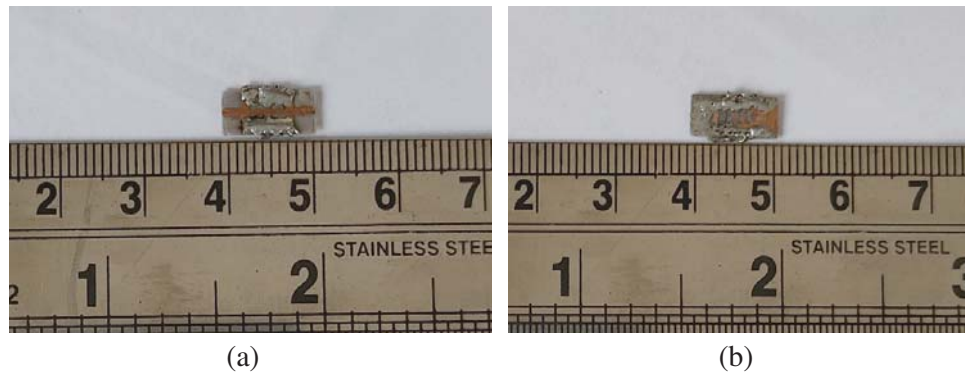
Figure 7. The Photographs of the fabricated dual-bandmm-wave BPF. (a) Top side view, and (b) bottom side view.
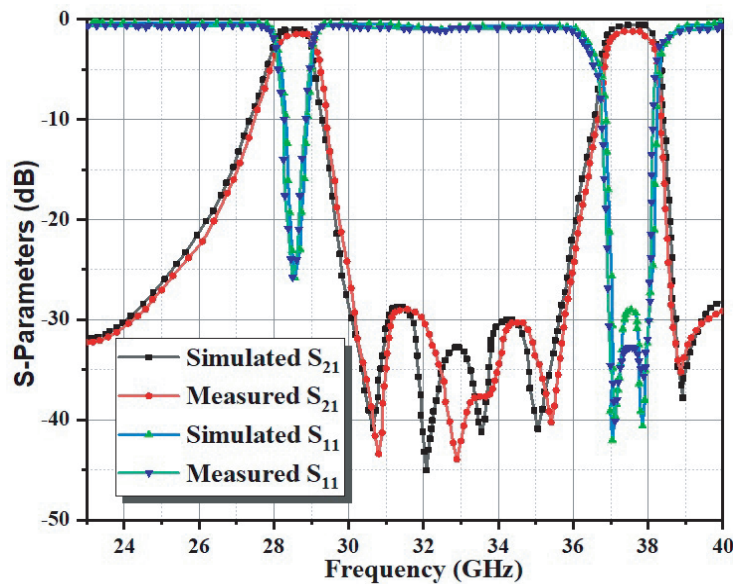
Figure 8. The full-wave measured and simulated results of the dual-band mm-Wave BPF.

Table 1. The detailed comparison of the different proposed and developed filters.

Ref.	Design Method	Centre Frequency	FBW%	Insertion Loss (dB)	Return Loss (dB)	Size ($\lambda_g \times \lambda_g$)
[20]	SIW	174	13.8	1.9	-	1.72×0.72
[21]	HLDR	36.35	15.7	0.95	21	1.35×1.59
[22]	SIW	38.2	8.4	1.7	14	2.64×1.04
[23]	SIW	33.03	10.1	1	11	3.2×1.33
[19]	Microstrip	33.5	4.2	0.85	17	1.5×0.6
Proposed work	SIW	28.3, 38.5	2.4, 3.4	01	28	0.82×0.45

Abbreviations used in table: *FBW = Fractional bandwidth, *SIW = Substrate integrated waveguide, *HLDR = Hybrid lumped and distributed resonators.

4. CONCLUSION

A dual-band mm-Wave BPF based on the DB-DGS SIW structure with the centre frequencies of 28.3 GHz and 38.5 GHz is proposed and fabricated. This dual-band mm-Wave BPF possess the attenuation, i.e., insertion loss of not more than 01 dB and the rejection attenuation (return loss) greater than 28 dB. In order to achieve the reconfigurability along the second passband, the geometric parameters are varied and optimized. Moreover, this filter produces three transmission zeros and two transmission poles in the stopband and the second passband, respectively. The simulated results of the filter are validated and found in good agreement. The compactness of this fabricated dual-band BPF covering frequency bands 28.3 GHz and 38.5 GHz with 3-dB fractional bandwidths of 2.4% and 3.4%, respectively makes this filter suitable for different 5G and millimeter-wave applications.

REFERENCES

1. Ali, M., F. Liu, A. Watanabe, P. M. Raj, V. Sundaram, M. M. Tentzeris, and R. R. Tummala, "First demonstration of compact, ultra-thin low-pass and bandpass filters for 5g small-cell applications," *IEEE Microwave and Wireless Components Letters*, Vol. 28, No. 12, 1110–1112, 2018.

2. Bhat, Z. A., J. A. Sheikh, R. Rehman, S. A. Parrah, M. U. Amin, and S. D. Khan, "Compact microstrip bandpass filter using stepped-impedance resonators and stepped-lumped resonators for 5G Wi-Fi and WLAN applications," *2019 International Conference on Power Electronics, Control and Automation (ICPECA)* 1–4, IEEE, November 2019.

3. Dong, K., J. Mo, Y. He, Z. Ma, and X. Yang, "Design of a millimeter-wave dual-band bandpass filter using SIW dual-mode cavities," *2016 IEEE MTT-S International Wireless Symposium (IWS)* 1–3, IEEE, March 2016.

4. Sofi, I. B. and A. Gupta, "A survey on energy efficient 5G green network with a planned multi-tier architecture," *Journal of Network and Computer Applications*, Vol. 118, 1–28, 2018.

5. Tharani, D., R. K. Barik, Q. S. Cheng, K. Selvajyothi, and S. S. Karthikeyan, "Compact dual-band SIW filters loaded with double ring D-shaped resonators for sub-6 GHz applications," *Journal of Electromagnetic Waves and Applications*, Vol. 35, No. 3, 1–14, 2020.

6. Dong, Y. and T. Itoh, "Miniaturized dual-band substrate integrated waveguide filters using complementary split-ring resonators," *2011 IEEE MTT-S International Microwave Symposium*, 1–4, IEEE, June 2011.

7. Senior, D. E., X. Cheng, M. Machado, and Y. K. Yoon, "Single and dual band bandpass filters using complementary split ring resonator loaded half mode substrate integrated waveguide," *2010 IEEE Antennas and Propagation Society International Symposium*, 1–4, IEEE, July 2010.

8. Dong, Y. D., T. Yang, and T. Itoh, "Substrate integrated waveguide loaded by complementary split-ring resonators and its applications to miniaturized waveguide filters," *IEEE Transactions on Microwave Theory and Techniques*, Vol. 57, No. 9, 2211–2223, 2009.

9. Chen, X. P., K. Wu, and Z. L. Li, "Dual-band and triple-band substrate integrated waveguide filters with Chebyshev and quasi-elliptic responses," *IEEE Transactions on Microwave Theory and Techniques*, Vol. 55, No. 12, 2569–2578, 2007.

10. Miao, M. and C. Nguyen, "A novel multilayer aperture-coupled cavity resonator for millimeter-wave CMOS RFICs," *IEEE Transactions on Microwave Theory and Techniques*, Vol. 55, No. 4, 783–787, 2007.

11. Wang, J., Y. Guan, H. Yu, N. Li, S. Wang, C. Shen, and G. Zhang, "Transparent graphene microstrip filters for wireless communications," *Journal of Physics D: Applied Physics*, Vol. 50, No. 34, 34LT01, 2017.

12. Liu, L., Q. Fu, F. Liang, and S. Zhao, "Dual-band filter based on air-filled SIW cavity for 5G application," *Microwave and Optical Technology Letters*, Vol. 61, No. 11, 2599–2606, 2019.

13. Rogla, L. J., J. Carbonell, and V. E. Boria, "Study of equivalent circuits for open-ring and split-ring resonators in coplanar waveguide technology," *IET Microwaves, Antennas & Propagation*, Vol. 1, No. 1, 170–176, 2007.

14. Ahn, D., J. S. Park, C. S. Kim, J. Kim, Y. Qian, and T. Itoh, "A design of the low-pass filter using the novel microstrip defected ground structure," *IEEE Transactions on Microwave Theory and Techniques*, Vol. 49, No. 1, 86–93, 2001.

15. Huang, Y., Z. Shao, and L. Liu, "A substrate integrated waveguide bandpass filter using novel defected ground structure shape," *Progress In Electromagnetics Research*, Vol. 135, 201–213, 2013.

16. Chen, R. S., S. W. Wong, L. Zhu, and Q. X. Chu, "Wideband bandpass filter using U-slotted Substrate Integrated Waveguide (SIW) cavities," *IEEE Microwave and Wireless Components Letters*, Vol. 25, No. 1, 1–3, 2014.

17. Ahn, D., J. S. Park, C. S. Kim, J. Kim, Y. Qian, and T. Itoh, "A design of the low-pass filter using the novel microstrip defected ground structure," *IEEE Transactions on Microwave Theory and Techniques*, Vol. 49, No. 1, 86–93, 2001.

18. Yoon, J. S., J. G. Kim, J. S. Park, C. S. Park, J. B. Lim, H. G. Cho, and K. Y. Kang, "A new DGS resonator and its application to bandpass filter design," *2004 IEEE MTT-S International Microwave Symposium Digest (IEEE Cat. No. 04CH37535)*, Vol. 3, 1605–1608, IEEE, June 2004.

19. Bhat, Z., J. Sheikh, S. Khan, R. Rehman, and S. Ashraf, "Compact and novel coupled line microstrip bandpass filter based on stepped impedance resonators for millimetre-wave communications," *Frequenz*, 2021, https://doi.org/10.1515/freq-2020-0156.

20. Li, Y., L. A. Yang, L. Du, K. Zhang, and Y. Hao, "Design of millimeter-wave resonant cavity and filter using 3-D substrate-integrated circular waveguide," *IEEE Microwave and Wireless Components Letters*, Vol. 27, No. 8, 706–708, 2017.

21. Shen, G., W. Che, and Q. Xue, "Compact microwave and millimeter-wave bandpass filters using LTCC-based hybrid lumped and distributed resonators," *IEEE Access*, Vol. 7, 104797–104809, 2019.

22. Li, J., Y. Huang, H. Wang, P. Wang, and G. Wen, "38-GHz SIW filter based on the stepped-impedance face-to-face E-shaped DGSs for 5G application," *Microwave and Optical Technology Letters*, Vol. 61, No. 6, 1500–1504, 2019.

23. Parment, F., A. Ghiotto, T. P. Vuong, J. M. Duchamp, and K. Wu, "Ka-band compact and high-performance bandpass filter based on multilayer air-filled SIW," *Electronics Letters*, Vol. 53, No. 7, 486–488, 2017.